PAPER 5 (SESSION I)

A study of crack tip deformation and a derivation of fracture energy

D. P. ROOKE and F. J. BRADSHAW

Royal Aircraft Establishment, Farnborough, Hants, England

Summary

Thin sheets of two aluminium alloys with central transverse fatigue cracks were subjected to increasing static loads until fracture occurred. Replicas were made under load of the surface deformation round the tips of the growing cracks and the strain fields deduced. Assuming a state of plane stress and that the stress throughout the plastic zone was equal to the Mises flow stress, the energy stored in the plastic zone was derived. Hence R, the resistance to crack growth, could be estimated at different load levels.

It was found that the strains in the plane of the sheet parallel to the tensile axis were an order of magnitude larger than the strains perpendicular to it. Comparisons were made with earlier work. The experimental R was compared with that obtained from orthodox fracture mechanics theory.

Most data was obtained on an Al Cu alloy (DTD646). Similar measurements were made in less detail on an Al Zn alloy (DTD687, cladding removed).

Introduction

According to the usual Griffith-Irwin description of energy balance during fracture, as a crack propagates in a loaded sheet the rate at which energy is released from the elastic strain field must be greater than or equal to the local work necessary to maintain crack growth. Fracture mechanics is concerned with calculating the strain energy release rate ($\mathcal{G}$); at the onset of crack propagation $\mathcal{G}$ will be just equal to R – the so called resistance of the material to crack growth. For thin sheets in nearly plane stress conditions there is normally a period of stable crack growth as the stress (σ) rises before fracture occurs. During this period of stable growth there is assumed to be a continuous balance between $\mathcal{G}$ and R. A possible description of this energy balance was first suggested by Krafft [1] and recently in more detail by Broek [2] (see also discussion to paper by Havner and Glassco [3]); a schematic representation is shown in Fig. 1. Several R curves have been deduced from measurements of stable crack growth [4, 5]. A necessary modification to this description is described later.

We report, in this paper, on measurements of the plastic displacements (δ) near to the crack tip. Then R is calculated directly from the work (W) necessary to deform plastically the region round the crack tip (the energy required to form new crack surfaces is of course negligible). The assumptions are made that there is a constant flow stress throughout the plastic region and that, since there is a state of plane stress, the strains in the interior of the sheet are the same as those on the surface.

Using a replica technique, measurements of surface displacements under load were made at various crack lengths. The calculated work rate is compared with R curves derived from fracture mechanics theory. The observed strain distributions are compared with those obtained by previous workers [6, 7] but it is difficult to do detailed comparisons since the photoelastic techniques used by others could not resolve the large strains which occur close to the crack tip. Also, some of the measurements were on specimens that had been unloaded [7] and it is known that considerable reverse plastic flow occurs on unloading [8]. Some numerical data obtained from the theoretical model by Swedlow, Williams and Yang [9] was compared with the experimentally measured strains. Use of the replica technique enables measurements to be taken in the loaded state and allows resolution of much larger strains.

Method

Two sheet aluminium alloys were used. One was an Al Cu alloy DTD646, the other an Al Zn Mg alloy DTD687. Approximately equivalent American specifications are 2014-T6 and 7075-T6. Tensile properties were respectively: ultimate tensile strength – 66,700 and 86,700 lbf in^{-2}: 0·2% proof stress – 59,400 and 79,500 lbf in^{-2}: Young's modulus – $1{\cdot}06\times10^{7}$ and $1{\cdot}02\times10^{7}$ lbf in^{-2}: elongation on one inch gauge length – 10·5% for both. Any cladding originally present was machined off and the final thicknesses of the sheets were respectively 0·033 and 0·032 in. Specimens 4 in wide by 9 in long (7 in free length) were made with central transverse saw cuts 0·625 in long. The surfaces of the sheets near the saw cuts were mechanically polished and scribed with suitable reference grid lines for subsequent strain measurement. Fatigue cracks were then grown from the ends of the saw cuts at a stress of 4400 ± 3600 lbf in^{-2} to provide a total crack length of 1 in.

Various methods of surface replication were tried; the Hickson method [10] was the one finally adopted. This makes use of a simple gun which fires a pre-heated platen containing an easily fusible alloy at the area of interest. The platen cools while adhering to the specimen, the solidified fusible alloy replicates the strained region and the platen is then removed for detailed study. Fig. 2 gives an indication of the method. A replica of the strained surface and one of the unstrained surface are placed side by side under a special comparator microscope and the relative displacements of the reference grid lines are measured. In addition, if required, displacements normal to the specimen surface can be obtained by tracking over the replica with a 'Talysurf' profile measuring instrument. The replica hardness and stylus pressure was such that this tracking caused negligible damage to the replica. These techniques pro-

vided a very simple and quick method of recording surface displacements under load to an accuracy of a few microns. The only modifications to the standard procedure necessary were those to reduce the effect of the impact of the platen on the loaded specimen. Near the failure load such impacts could occasionally cause the cracks to grow slightly. To eliminate this the sheet was backed by a movable anvil covered with thin plastic tape and the striking velocity of the platen was reduced with friction dampers.

The loading of the specimen was tensile, normal to the crack, and was increased by stages to allow for crack tip replication. A relatively soft tensile machine was used so that there was no fall in load as the crack advanced. To permit extrapolation of the records to the point of failure separate specimens were loaded similarly. Crack lengths and loads at failure were recorded. The time from start of loading to fracture was about one hour. To prevent any tendency for the sheet to buckle under load lubricated supports were mounted transversely on the specimen, though these were probably not necessary.

Results

The fatigue crack surfaces prior to static loading were normal to the sheet surface in both alloys. As the static load was increased the growing crack surfaces rotated into single planes at 45° to the sheet surface. The 45° plane was reached for both alloys by the time the crack had grown a distance about equal to the sheet thickness; the observed plastic zones were then about 4 times (646 alloy) and 2 times (687 alloy) the sheet thickness.

Replicas were taken of both crack ends, on both sides of the sheet, as soon as they started to grow. All of these were used to give an average value of Δa, the static crack growth increment on the starting half-length, a_0. The total half length, a, equals $a_0 + \Delta a$. Both crack ends behaved similarly and only one was examined in detail. The strain distributions and crack opening displacements on both sides of the sheet were measured and, apart from the reversed symmetry due to the 45° crack surface, were found to be very little different.

Taking the fatigue crack tip as origin, with x, y coordinates in the plane of the sheet parallel and perpendicular to the crack, ϵ_x and ϵ_y the measured surface strains and ϵ_z the strain normal to the surface, it was observed that ϵ_x was much less than ϵ_y. Except possibly very near the crack tip, ϵ_x was always negative. If with the 646 alloy we assume that the plastic strains ϵ_x^p and ϵ_y^p are equal to the measured strains less an elastic strain of 0;6% (= 0;2% proof stress/modulus) then ϵ_x^p was always less than 5% of ϵ_y^p. The variation of ϵ_x^p and ϵ_x^p with y close to the crack tip is shown in Fig. 3. With the 687 alloy, taking a limiting

elastic strain of 0·8%, ϵ_z^p was zero. Thus for both alloys it was assumed in the calculation of the fracture energy that the plastic deformation was one of (y, z) plane strain. With constant volume deformation ϵ_z^p would be equal to $-\epsilon_y^p$. Talysurf records of the 646 alloy replicas were analysed and it was found that ϵ_z^p, where it was appreciable, was indeed equal and opposite to ϵ_y^p within the limits of measurement error. Talysurf records near the periphery of the plastic zone however proved to be an unreliable indication of ϵ_z^p since small changes in the angle of the sheet surface made it difficult to define the contour of zero plastic strain. For this reason most measurements were made of y displacements.

Figs. 4 and 5 give typical contours of ϵ_y^p deduced from measurements on one side of the sheet only, at stresses near to fracture. The slight lack of symmetry due to the 45° crack angle can be seen. The plastic zone of the 646 alloy proved to be larger at the highest stresses than the standard replica size and so the $\epsilon_y^p = 0$ contour was not covered everywhere. However coverage was sufficient to allow for some extrapolation. The fan shaped plastic zones shown in Figs. 4 and 5 were typical of the zones observed at all stress levels studied.

Crack opening displacements (C.O.D.) at the fatigue crack tip were also obtained from the replicas. The simple formula proposed by Wells [11] (C.O.D. $= 4\mathcal{G}/(\pi\sigma_y)$, where σ_y is the yield stress – equal to the 0·2% proof stress) gave a very good prediction of the observed displacements in both alloys. These are shown, together with values of a and the area of the plastic zone as defined by $\epsilon_y^p = 0$ contour, in Fig. 6 at different stress levels below fracture.

Considering the variation of ϵ_y^p with y, for different distances ahead of the crack tip, the ϵ_y^p maxima were found to be directly ahead of the growing tip. These maxima (average of both sides of the sheet) are shown in Figs. 7 and 8 as a function of $(x - \Delta a)$.

Fracture energy

As the crack grows stably under an increasing load the energy dissipated in plastic deformation derives from two sources; the strain energy released by the elastic field due to the increase in crack length and the external work done in increasing the load. The detailed energy balance has been discussed at length by Havner and Glassco [3]. The two sources of energy dissipation can be combined by considering the plastic zone at the tip of crack to be equivalent to an effective increase in crack length; this notion is of course common in fracture mechanics [12]. Thus an increase in the size of the plastic zone due to an increase in stress is equivalent to an increase in the effective half-crack length (a'). At a given stress a' is defined by

$$a' = a + mr_p \tag{1}$$

where m is a constant and r_p, a plastic zone 'radius', is given by

$$r_p = K^2/(2\pi\sigma_y^2) = E\,\mathcal{G}/(2\pi\sigma_y^2) \tag{2}$$

where K is the stress intensity factor and E is Young's Modulus. Irwin [13] has deduced that m lies between 0·75 and 1·3; he suggests $m = 1$ agrees best with experimental data and this value has been used in the present work. Thus the total work (W) done in plastic deformation must be considered as a function of a' and the rate of change of $W(a')$ with area of effective crack is R. Therefore during stable crack growth,

$$\frac{1}{t} \cdot \frac{dW(a')}{da'} = R = G(a'),$$

where t is the sheet thickness. Hence Fig. 1 should be modified; $\mathcal{G}$ and R are better plotted as functions of a', not a. Such a presentation is even more appropriate to plane strain where there is no crack growth up to the 'pop-in' instability. R is a function of $(a_0 + r_p)$ only.

The strain energy release rate was calculated from

$$\mathcal{G}(a') = [K(a')]^2/E \tag{4}$$

with $K(a')$ calculated according to the formula of Brown and Srawley [14] using an iterative procedure. In order for valid calculations of $\mathcal{G}$ to be made it is necessary that $r_p \ll a$. In DTD646, at the highest stress, the plastic zone size was becoming comparable with the crack length and the net stress comparable with σ_y; hence $\mathcal{G}$ may, at this stress, be appreciably in error.

Making use of the fact that ϵ_x^p was effectively zero, the total plastic work done in producing a plastic zone was simply obtained by considering the zone as consisting of thin elements parallel to the y axis, ending at the zero plastic strain contour, which had been extended under a uniform stress by amounts equal to the displacements of their ends. The stress is assumed to be constant and equal to $1{\cdot}15\sigma_y$. The factor of 1·5 arises from assuming a Mises yield criterion for a material constrained in plane plastic strain. Because the $\epsilon_y^p = 0$ contour far from the crack tip was not well defined in the 646 alloy, the energies contained in the two zones defined by $\epsilon_y^p = 1{\cdot}0\%$ and $\epsilon_y^p = 0{\cdot}5\%$ were calculated and that in $\epsilon_y^p = 0$ obtained by extrapolation; these were denoted by W_1, $W_{0.5}$ and W_0. For the 687 alloy only W_0 was calculated from its smaller well defined $\epsilon_y^p = 0$ boundary. The above derivation ignores any work due to plastic shearing. In the 687 alloy all the shear strains observed in the xy-plane were within the elastic range. In the 646 alloy plastic shear strains (γ_{xy}^p) were at most a few per cent of ϵ_y^p except in a small region about 0·02 in wide either side of the growing crack. This region is about 2% of the area

of the plastic zone and contains about 5% of the plastic work. Since the maximum value of $\gamma_{xy}{}^p/\epsilon_y{}^p$ is $\sim 0{\cdot}7$ and the contribution to the energy is proportional to $(\gamma_{xy}{}^p/\epsilon_y{}^p)^2$ the error in the total energy due to ignoring shear strains is very small. In fact 60% of the plastic work is contained in the region defined by $0 \leqslant \epsilon_y{}^p \leqslant 1{\cdot}0\%$.

The calculated W's were plotted as functions of a' and the rate dW/da' computed. R, which is $(dW/da')/t$, is compared with $\mathscr{G}$ in Figs. 9 (a) and 9 (b) for the two alloys ($R_0 = (dW_0/da')/t$ etc. in the 646 results). The upper portions of the R_0 and $R_{0{\cdot}5}$ curves are shown as broken lines since they are extrapolations. R for the 687 alloy is shown as a band. The spasmodic type of crack growth which occurs in this alloy introduced a scatter in the results. The critical effective crack length (a_c') and the value of $\mathscr{G}_c$ shown were obtained from the further tests on similar specimens simply loaded to failure.

Discussion and conclusions

Crack opening displacements

The simple theoretical derivation of C.O.D., in terms of $\mathscr{G}$, by Wells [11], has been shown in Fig. 6 to agree well, for both alloys, with that measured at the tip of the fatigue crack.

Strain measurements

The deformation within the plastic zones of both alloys has been shown to be effectively one of (y, z) plane plastic strain. In Figs. 7 and 8 the ϵ_y strains ahead of the crack plotted on log-log scales lie close to the straight lines which have been drawn of slope -1. From this it can be seen that the strains are approximately proportional to x^{-1} except very close to the tip (i.e. $x \leqslant t$). Hult and McClintock [15] have shown that in a perfectly elastic – plastic material subject to pure shear the strain ahead of the crack is proportional to x^{-1}; in a perfectly elastic material the strain is proportional to $x^{-1/2}$. Similar results have been obtained by others [6, 7]. Comparing the results in Fig. 7 for $\sigma = 30{,}300$ lbf in^{-2} with those in Fig. 8 for $\sigma = 30{,}500$ lbf in^{-2} it is seen that the strains in the 646 alloy are $\sim 50\%$ higher than those in the 687 alloy at the same stress; at failure they were roughly 100% higher despite the same elongation to failure in a tensile test ($10{\cdot}5\%$ on a 1 in gauge).

The calculations of Swedlow *et al.* [9] are not strictly comparable with the experimental results since their model stress-strain curve is different from our experimental ones. However the Young's moduli are approximately the same and the elastic limits for both of our alloys are approximately $2{\cdot}5$ times that used in the model. Scaling the model stresses up by this factor enables a rough comparison to be made. In Fig. 10 the experimental values of ϵ_y at the appropriate stresses are compared with the theoretical values of the difference in principal strains $(\epsilon_1 - \epsilon_2)$; since

$\epsilon_x, \gamma_{xy} \ll \epsilon_y$ we have $\epsilon_y \simeq \epsilon_1 \gg \epsilon_2$. There is fair agreement, but it would be desirable to repeat the calculations using the experimental stress-strain laws.

Comparison of R and $\mathscr{G}$

While the derivations of R and $\mathscr{G}$ are not sufficiently accurate to enable the shape of the R curve to be clearly defined the overall agreement between R and $\mathscr{G}$ is considered to be satisfactory and would justify a more thorough investigation (using larger test specimens for the 646 alloy). The marked reduction in the slope of the R_0 curve in the 646 alloy with increasing a may well be due to the errors in extrapolating the replica data. In addition to the uncertainties in R due to spasmodic crack growth in the 687 alloy there are larger experimental uncertainties in dW/da', than in the 646 alloy, since the variation in both W and a' is much less.

It is appreciated that the simplified strain pattern in the plastic zone which we have taken for convenience in calculating R would, if completely correct, offer no explanation for the fact that R increases as a increases even after the crack has rotated into the 45° plane. If we consider an element of material ahead of and very near to the crack path, then as the crack grows and the tip moves past or through this element the principal strains rotate about both the x and z axes and the strain pattern becomes more complex. With such a deformation history this element may fail at a higher stress or strain than one in front of a stationary crack. McClintock and Irwin [16] have shown that rotation of the stress direction can, in some cases, lead to a stable situation with a lowering of the strain ahead of the crack; an increase in applied stress is needed for further crack growth. Because an increase of R with a only appears to occur in thin sheets it should be the strain rotation about the x axis which is important. While these features are relevant when considering the origins of the stable growth we do not think that they are in our calculations of R.

Acknowledgements

We are grateful to K. Pearmain for assistance in much of the experimental work. Crown copyright, reproduced with the permission of the Controller, Her Majesty's Stationery Office.

References

1. KRAFFT, J. M., SULLIVAN, A. M. and BOYLE, R. W. 'Effect of dimensions on fast fracture instability of notched sheets' *Proc. Crack Propagation Symp.*, Cranfield, 1961, vol. 1, p. 8.
2. BROEK, D. 'The energy criterion for fracture of sheets containing cracks' *Appl. Mat. Res.*, vol. 4, p. 188, 1965.

3. HAVNER, K. S. and GLASSCO, J. B. 'On the energy balance criteria in ductile fracture' *Int. J. fracture Mech.*, vol. 2, p. 506, 1966.
4. BROEK, D. 'The effect of finite specimen width on the residual strength of light alloy sheet' NLR-TR M. 2152, National Aerospace Laboratory, The Netherlands, Sept. 1965.
5. CARMAN, C. M., ARMIENTO, D. F. and MARKUS, H. 'Crack resistance properties of high strength aluminium alloys' *Proc. 1st Int. Conf. on Fracture* (Sendai 1965), vol. 2, p. 995, 1966.
6. DIXON, J. R. and STRANNIGAN, J. S. 'Strain distributions around cracks in ductile sheets during loading and unloading' *J. mech. Engng. Sci.*, vol. 7, p. 312, 1965.
7. GERBERICH, W. W. 'Plastic strains and energy density in cracked plates' *Expl. Mech.*, vol. 4, p. 335, 1964.
8. BATEMAN, D. A., BRADSHAW, F. J. and ROOKE, D. P. 'Some observations on surface deformation round cracks in stressed sheets' Royal Aircraft Establishment Technical Note No. CPM.63, March 1964.
9. SWFDLOW, J. L., WILLIAMS, M. L. and YANG, W. H. 'Elastoplastic stresses and strains in cracked plates' *Proc. 1st Int. Conf. on Fracture* (Sendai 1965), vol. 1, p. 259, 1966.
10. HICKSON, V. M. 'A replica technique for measuring static strains' *J. mech. Engng. Sci.*, vol. 1, p. 171, 1959.
11. WELLS, A. A. 'Unstable crack propagation in metals: cleavage and fast fracture' *Proc. Crack Propagation Symp.*, Cranfield 1961, vol. 1, p. 210.
12. ASTM Committee. 'Fracture testing of high-strength sheet materials' ASTM Bulletin, p. 29, Feb. 1960.
13. IRWIN, G. R. 'Plastic zone near a crack and fracture toughness' *Proc. 7th Sagamore Ordnance Materials Conference*, Syracuse University Research Institute, p. IV-63, 1960.
14. BROWN, W. F. and SRAWLEY, J. E. 'Plane strain crack toughness testing of high strength materials' ASTM Special Technical Publication No. 410, 1966.
15. HULT, J. A. H. and McCLINTOCK, F. A. 'Elastic-plastic stress and strain distributions around sharp notches under repeated shear' *9th Int. Congress of Applied Mechanics*, vol. 8, p. 51, 1957.
16. McCLINTOCK, F. A. and IRWIN, G. R. 'Plasticity aspects of fracture mechanics' *Fracture Toughness testing and its applications*, ASTM Special Technical Publication No. 381, p. 84, 1965.

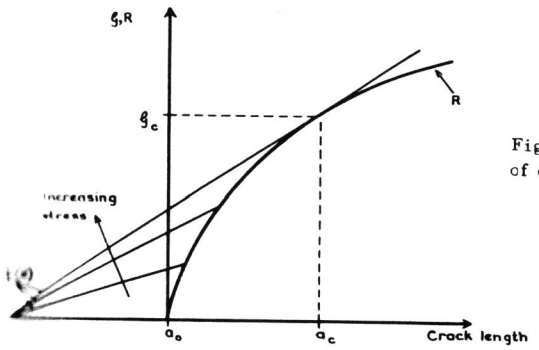

Fig. 1. Schematic representation of energy balance.

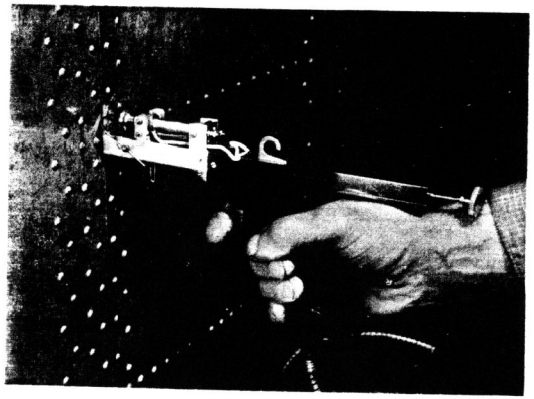

Fig. 2. A Hickson replica gun in use.

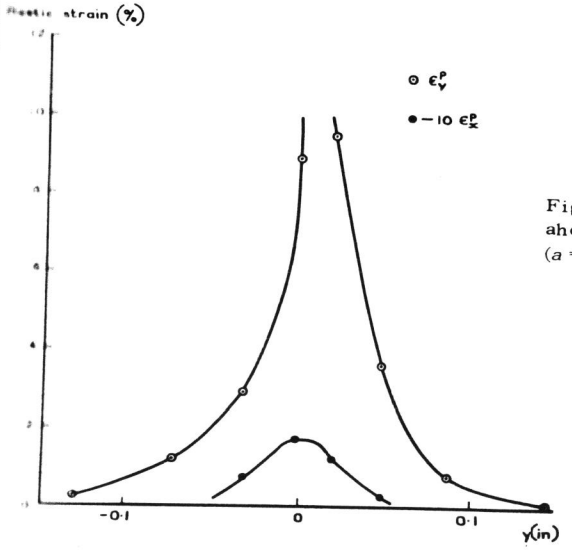

Fig. 3. Plastic strains 0·004 in ahead of the crack in DTD646 (a = 0·617 in, σ = 40,200 lbf in^{-2}).

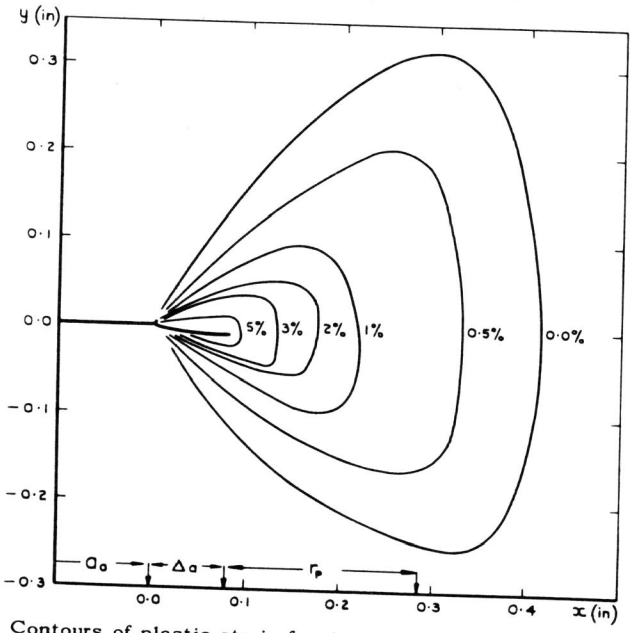

Fig. 4. Contours of plastic strain for the DTD646 specimen (a = 0·574 in, σ = 39,000 lbf in^{-2}).

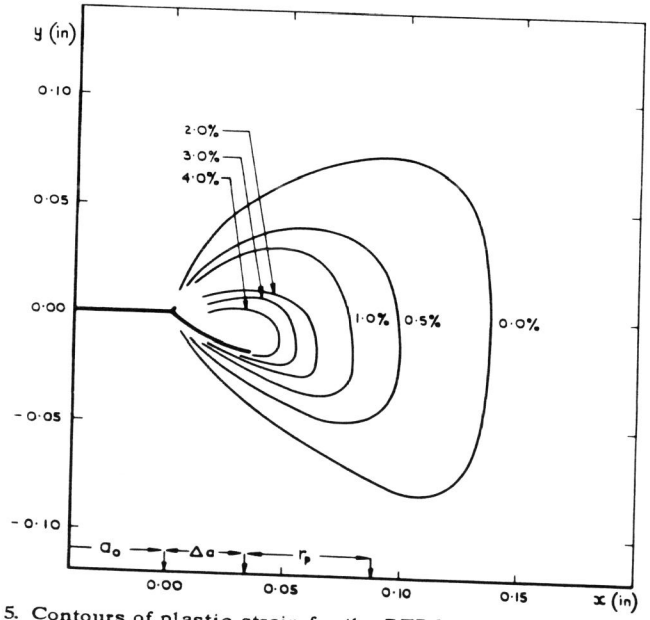

Fig. 5. Contours of plastic strain for the DTD687 specimen (a = 0·530 in, σ = 32,200 lbf in ^{2}).

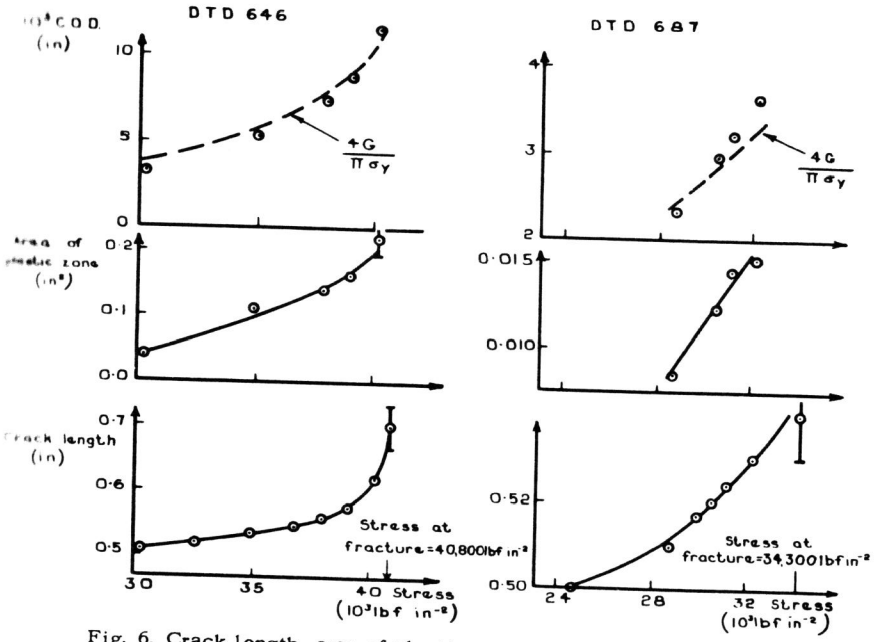

Fig. 6. Crack length, area of plastic zone and C.O.D. vs. stress.

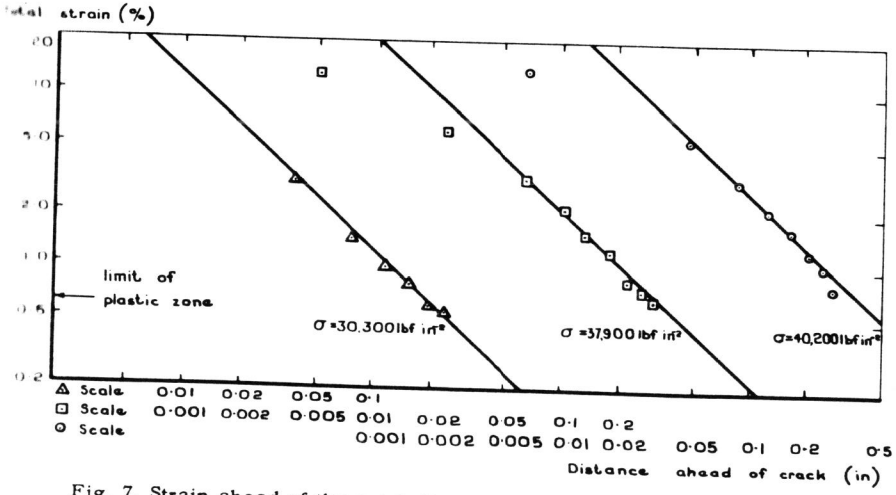

Fig. 7. Strain ahead of the crack tip at various stresses in DTD646.

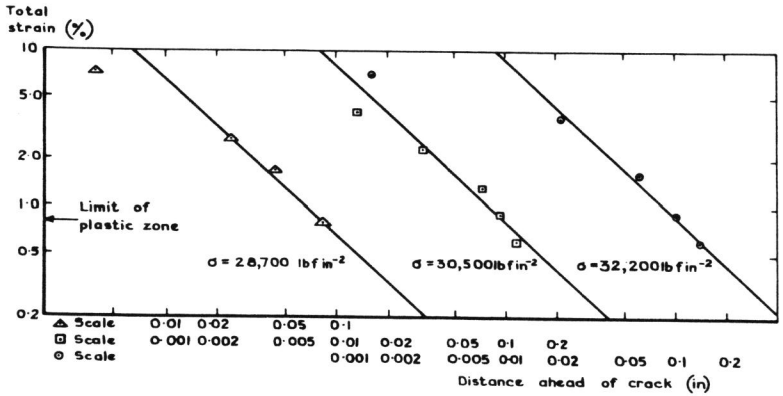

Fig. 8. Strain ahead of the crack tip at various stresses in DTD687.

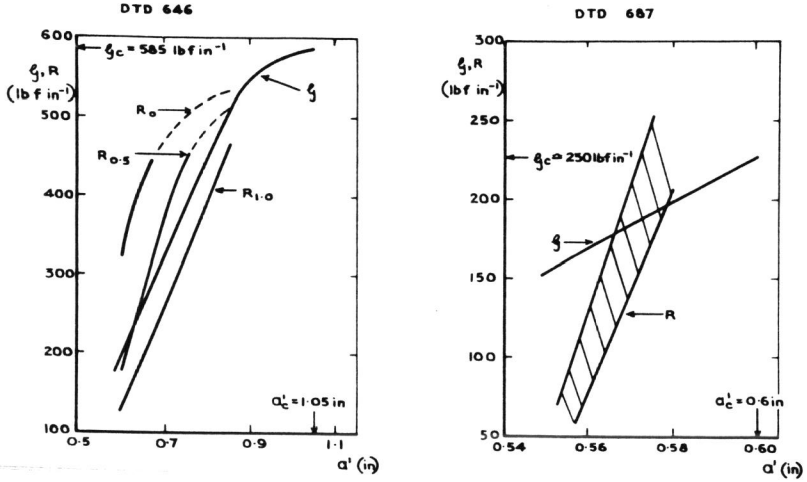

Fig. 9 (a). Comparison of R and $\mathcal{G}$ for DTD646.

Fig. 9 (b). Comparison of R and $\mathcal{G}$ for DTD687.

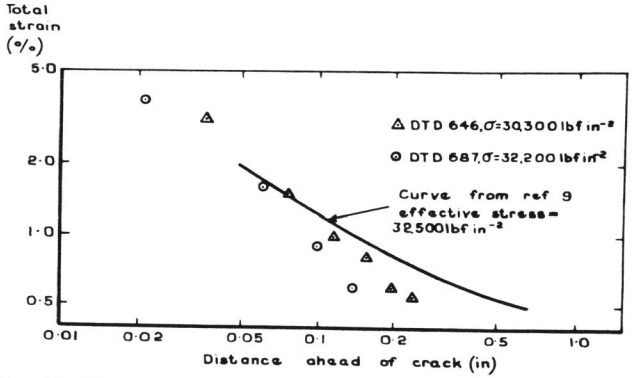

Fig. 10. Strain ahead of the crack (experimental and theoretical).